GIScience & Remote Sensing

ISSN: 1548-1603 (Print) 1943-7226 (Online) Journal homepage: www.tandfonline.com/journals/tgrs20

Airborne lidar intensity correction for mapping snow cover extent and effective grain size in mountainous terrain

Chelsea Ackroyd, Christopher P. Donahue, Brian Menounos & S. McKenzie Skiles

To cite this article: Chelsea Ackroyd, Christopher P. Donahue, Brian Menounos & S. McKenzie Skiles (2024) Airborne lidar intensity correction for mapping snow cover extent and effective grain size in mountainous terrain, GIScience & Remote Sensing, 61:1, 2427326, DOI: 10.1080/15481603.2024.2427326

To link to this article: https://doi.org/10.1080/15481603.2024.2427326

Published online: 12 Nov 2024.

GISCIENCE & REMOTE SENSING
2024, VOL. 61, NO. 1, 2427326
https://doi.org/10.1080/15481603.2024.2427326

Taylor & Francis
Taylor & Francis Group

Airborne lidar intensity correction for mapping snow cover extent and effective grain size in mountainous terrain

Chelsea Ackroyd[a], Christopher P. Donahue[b,c,d], Brian Menounos[b,c,e] and S. McKenzie Skiles[a]

[a]School of Environment, Society & Sustainability, University of Utah, Salt Lake City, UT, USA; [b]Department of Geography, Earth, and Environmental Sciences, University of Northern British Columbia, Prince George, BC, Canada; [c]Hakai Institute, Cambell River, BC, Canada; [d]Bridger Photonics, Inc, Bozeman, MT, USA; [e]Geological Survey of Canada Pacific, Natural Resources Canada, Sidney, BC, Canada

ABSTRACT

Differentially mapping snow depth in mountain watersheds from airborne laser altimetry is a valuable hydrologic technique that has seen an expanded use in recent years. Additionally, lidar systems also record the strength of the returned light pulse (i.e. intensity), which can be used to characterize snow surface properties. For near-infrared lidar systems, return intensity is relatively high over snow and inversely related to the effective grain size, a primary control on snow albedo. Raw intensity is also sensitive to laser range and incidence angle, however, and requires a correction for snow property retrieval that is especially pertinent in mountainous terrain. Here, we describe a workflow to correct the intensity using the plane trajectory, lidar scan angle, and lidar-derived topography. As a proof of concept for snow retrievals, we apply the workflow to an airborne 1064 nm lidar flight over a snow-covered mountain basin in the Colorado Rockies. Corrected intensity was empirically related to reflectance before delineating snow extent and retrieving grain size. Relative to the traditional snow classification derived from optical imagery, the lidar-derived snow extent covered 5.4% more area due to the fine resolution point cloud and absence of shadows common in optical imagery. The lidar-derived grain size retrievals had a MAE of 32 µm compared to those from field spectroscopy, which translated to a 1% error in snow albedo. We found high incidence angles yielded an overcorrection in intensity that introduced a high bias in the grain size distribution and, therefore, suggest using an incidence angle threshold (40°). Developing methods specifically for quantitative snow surface property retrievals from lidar intensity is timely and relevant as aerial lidar is increasingly being used to map snow depth for hydrologic and cryospheric studies.

ARTICLE HISTORY
Received 28 March 2024
Accepted 4 November 2024

KEYWORDS
Lidar; lidar intensity; snow; snow grain size; topographic correction

1. Introduction

Airborne laser scanning (ALS) applications within snow hydrology have increased exponentially in recent decades, with most studies focused primarily on characterizing snow volume, including snow depth, snow redistribution, and avalanche movement (Anttila et al. 2016; Bhardwaj et al. 2016; Helfricht et al. 2014; Hood and Hayashi 2010; T. H. Painter et al. 2013; Prokop 2008; Vionnet et al. 2021). Snow depth mapping is commonly conducted by differencing two geo-registered topographies of the same location: one with snow ("snow on") and the other snow-free ("snow off") (T. H. Painter et al. 2016). The temporal differencing approach can provide an observation of snow depth with sub-decimeter vertical accuracy and a fine spatial resolution across entire watersheds (Deems, Fassnacht, and Elder 2006; Deems, Painter, and Finnegan 2013; Mott, Schirmer, and Lehning 2011).

In addition to snow depth and distribution, lidar can also be used to map surface optical properties by leveraging the intensity measurement, or the ratio of the strength of the return signal relative to that of the emitted pulse (Song et al. 2002). Theoretically, lidar intensity should vary with the reflectivity of a surface, allowing lidar to be both a spatial and a spectral instrument (Antonarakis, Richards, and Brasington 2008). Raw intensity, however, is not directly usable for retrievals. The absolute magnitude of the values varies with factors that include transmitted power, laser pulse repetition rate, range (e.g. the distance between the sensor and the surface), atmospheric conditions, topography of the study area, scan angle, footprint size, beam divergence, and surface composition (Bretagne, Dassonvalle, and Caron 2018; Kashani et al. 2015). Although various approaches

CONTACT Chelsea Ackroyd chelsea.ackroyd@utah.edu

exist for intensity correction, there is no standardized method and, thus, these data remain unexploited (Lang and McCarty 2009; Sanchiz-Viel et al. 2021; Song et al. 2002; Yan and Shaker 2018).

To translate intensity into an analysis-ready product, correction for range and incidence angle is of primary importance (Jutzi and Gross 2009; Kaasalainen et al. 2011; Sanchiz-Viel et al. 2021). An increase in the range extends the travel path of the laser pulse, exacerbating the energy loss due to beam divergence and considerably reduces the number of returns. Relatedly, an increase in range and incidence angle enlarges the footprint of a given laser pulse, lengthening travel time for the laser pulse and weakening the return intensity (Goodwin, Coops, and Culvenor 2006). Accounting for these parameters is especially critical over snow-covered mountainous watersheds, where the topography produces high variability in both range and incidence angle (Currier et al. 2019; Deems, Painter, and Finnegan 2013; Hartzell et al. 2015; Soudarissanane et al. 2009).

Topographic complexity may confound one-to-one mapping between return intensity and snow property retrieval, but these challenges can be overcome. Lidar sensors selected for monitoring snow typically operate in the near-infrared (Baltsavias 1999; Goodwin, Coops, and Culvenor 2006), where light penetration is relatively shallow (~1 cm), and snow is relatively bright (Deems, Painter, and Finnegan 2013). Previous studies delineated seasonal snow on a glacier surface from lidar intensity (Arnold et al. 2006; Prantl et al. 2017), whereas others used intensity to characterize snow, ice, rock, and water across a glacial region in Norway (Lutz, Geist, and Stötter 2003).

In addition to surface classification, variation in lidar intensity should relate to the effective grain size of snow, a surface optical property and primary control on snow albedo (Warren 1982). In the near-infrared portion of the electromagnetic spectrum, snow reflectivity is inversely related to the photon path length through ice, commonly characterized as an effective grain radius or specific surface area (SSA) (Warren 1982). Generally, as snow grains round and grow over time due to snow metamorphism, the effective grain size increases. Nolin (1998) and Yang et al. (2017) proposed a proof of concept for deriving snow grain size from the Geoscience Laser Altimeter System (GLAS) onboard the Ice, Cloud, and land Elevation Satellite (ICESat), although neither study could validate retrievals. At a finer scale, Kaasalainen, Kaartinen, and Kukko (2008) attributed variation in terrestrial lidar intensity over snow to grain size but noted that it was a qualitative assessment that could be further refined. For the remainder of the paper, we will refer to effective grain size simply as grain size.

Here, we present a method to correct lidar intensity at 1064 nm for range and incidence angle. To demonstrate this methodology, we applied the correction to a lidar flight over a snow-covered mountain watershed in Colorado and related the corrected intensity to reflectance, from which snow extent was delineated and grain size retrieved. The snow properties from lidar intensity were assessed against traditional retrieval approaches (i.e. snow extent from imagery and grain size from field spectroscopy). Retrieving snow extent and grain size from lidar intensity optimizes the full lidar dataset and provides a useful supplement to established methods with the added benefits of an active sensor.

2. Methods

2.1. Data

The lidar dataset used in our study originated from an airborne Riegl Q1560 dual laser scanner flown aboard a King Air A90 as a component of the Airborne Snow Observatory (ASO), a now complete NASA-JPL project (T. H. Painter et al. 2016). The acquisition occurred on 21 February 2017 over the Senator Beck Basin Study Area (SBBSA; Landry et al. 2014) in the San Juan Mountains, CO, as part of the NASA SnowEx campaign (Year 1; Figure 1a). The Riegl Q1560 is a 1064 nm, dual laser scanner with a system scan angle of 60° (±30° from nadir). Each flightline included 50% overlap, with the total survey area flown in a double overlap "checkerboard" flight pattern (10 flight lines in each direction; 4× lidar coverage) across a larger domain encompassing SBBSA, which was subset to the eight flight lines that cover the basin (Figure 1b).

The lidar sensor collected return signals at a pulse repetition rate of 400 kHz per laser and at 100% power. The flight altitude was 5,182 m (17,000 ft) above sea level (asl) with ground elevations in the study area spanning ~ 3345–4100 m (Figure 1c). At this elevation, beam divergence (0.25 mrad) for nadir laser pulses yield a footprint of ~1 m on flat

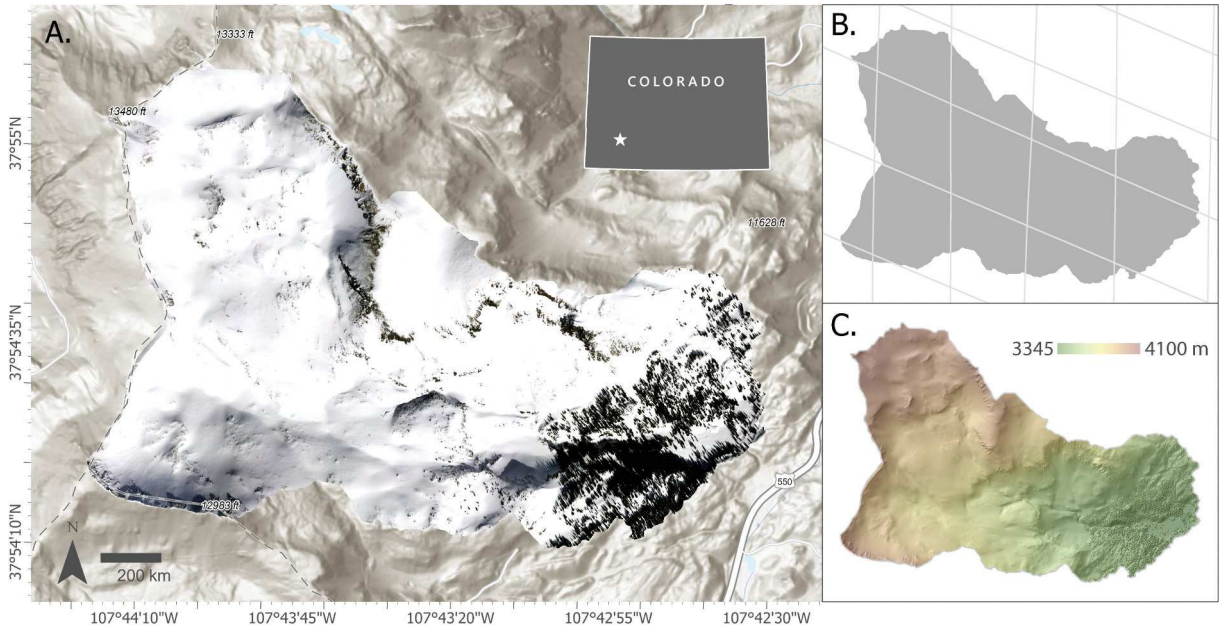

Figure 1. The study area is Senator Beck Basin in the San Juan Mountains, Colorado. (A) RGB orthomosaic from day of flight (B) Airborne Snow Observatory (ASO) flight lines on 21 February 2017 (C) Lidar-derived digital elevation model of the study area with values ranging from approximately 3345 – 4100 m. Sources for the basemap include ESRI, USGS, and NOAA.

terrain with increases in size proportionate to scan angle and topography (Deems, Painter, and Finnegan 2013). The survey commenced at 16:48 UTC (9:48 AM MST) and completed at 17:44 UTC (10:44 AM MST). Throughout the duration of this flight, clear skies existed in the survey area below the aircraft, while isolated cirrus clouds existed above the aircraft. The survey area experienced snowfall the previous day.

We collected in-situ spectral albedo and reflectance measurements with an ASD FS4 field spectrometer on the same day of overflight. The ASD FS4 samples the spectral range 350–2500 nm, with contiguous bands that are 3 nm (at 700 nm) to 10 nm (at 1400 and 2100 nm) at full width half maximum. The spectra are resampled and splined to 1 nm resolution, and the wavelength reproducibility and accuracy are 0.1 and 0.5 nm, respectively. Albedo measurements took place over both snow and snow-free targets (i.e. road asphalt adjacent to SBBSA). Reflectance transects took place over snow at two locations: an alpine meadow near the middle of the basin (Mid-basin, 3843 m) and the alpine study plot (Senator Beck Study Plot, 3716 m). Approximately 80 reflectance measurements, each with a ~25 cm footprint, were collected along ~2.5 m transects and georeferenced using locations from a handheld GNSS receiver (Trimble Geo), which had an uncertainty of 1–3 cm after post-processing. Mid-basin observations were being collected near the time the plane flew overhead (10:00 AM local time), and Senator Beck Study Plot measurements occurred later in the afternoon (2:00 PM local time). The albedo measurements were used as calibration data, referenced to convert corrected intensity to reflectance as described further in Section 2.2. The reflectance transects were used as assessment data; the effective snow grain size was retrieved from each spectral reflectance measurement and compared to the lidar-derived grain size as described in Section 2.3.

The imaging spectrometer (CASI-1500) on ASO was coincidentally recording at-surface reflectance continuously from 400 to 1040 nm (T. H. Painter et al. 2016). The imagery was processed by ASO to produce a basic land surface classification (e.g. snow, rock, vegetation, water) using band ratios, including the normalized difference snow index (NDSI, threshold > 0.86) for snow extent. The snow classification was used here to assess snow cover delineated from lidar intensity. Due to the decreasing signal-to-noise ratio and quality of spectral measurements past 900 nm, however, the instrument was not suitable for grain size retrievals (Soffer 2021). Additionally, because the spectral range does not extend to 1064 nm, a direct

spatial comparison between the lidar and imaging spectrometer reflectance was not possible.

2.2. Lidar intensity correction

2.2.1. Theory

Lidar operates under the same fundamental principles as radar, replacing radio waves with shorter wavelengths commonly found in the visible (520–-560 nm) and near-infrared (700–1400 nm) portion of the electromagnetic spectrum (Jelalian 1992; Sanchiz-Viel et al. 2021). A lidar instrument emits photons toward a target, the signal then encounters a surface, and a portion of the signal is backscattered toward the instrument's receiver. To begin the lidar intensity correction process, the factors that determine the intensity value first need to be understood by evaluating the radar equation:

$$P_r = \frac{P_t D_r^2}{4\pi R^4 \beta_t^2} \eta_{sys} \eta_{atm} \sigma \tag{2.1.}$$

$$\sigma = \frac{4\pi}{\Omega} \rho A_s \tag{2.2.}$$

where P_r is the received laser power (watts), P_t is the transmitted laser power (watts), D_r is the diameter of the receiver aperture (meters), R is the range or distance from the scanner to the surface (meters), β_t is the laser beam width (radians), η_{sys} and η_{atm} are the system and atmospheric attenuation, respectively, and σ includes the target characteristics of the cross-section, including Ω as the scattering solid angle (steradians), ρ as the target reflectance, and A_s as the target area (square meters; Höfle and Pfeifer 2007; Jelalian 1992). The raw intensity or the received laser power (P_r), therefore, is a reduction of the transmitted laser beam (P_t) in accordance with the instrumentation design, the geometric and reflectance properties of the scanned surface, as well as the atmospheric conditions.

Simplifying the radar equation (Equation 2.1) identifies which parameters have the highest impact on the received laser signal and could be leveraged to normalize the data. If a laser signal is assumed to encounter an individual surface with Lambertian reflectance, then the area of the target (A_s) is dependent upon the laser beam width (β_t) and range (R; Jelalian 1992):

$$A_s = \frac{\pi R^2 \beta_t^2}{4} \tag{2.3.}$$

This definition of the target area can be substituted when solving for the target characteristics of the cross-section (σ; Equation 2.2), which can refine the original radar equation (Equation 2.1) as follows:

$$\sigma = \pi \rho R^2 \beta_t^2 cos\alpha_i \tag{2.4.}$$

$$P_r = \frac{P_t D_r^2 \rho}{4R^2} \eta_{sys} \eta_{atm} cos\alpha_i \tag{2.5.}$$

where the $cos\alpha_i$ parameter is added to account for the incidence angle, or the angle between the incoming laser pulse and the surface normal (Baltsavias 1999; Höfle and Pfeifer 2007; Jelalian 1992; Figure 2). This modified equation indicates that the received laser pulse is proportional to the cosine of the incidence angle and has an inverse relationship with the squared range (Höfle and Pfeifer 2007).

The remaining parameters are primarily inherent to a lidar system and can be assumed to remain constant during overflight, including the transmitted laser signal, the receiver aperture diameter, and the systematic attenuation (Höfle and Pfeifer 2007). Although the atmospheric attenuation is a vital parameter, the strength of its effect on the received signal is mainly dependent upon the range (Höfle and Pfeifer 2007). Thus, the literature suggests that the range and the incidence angle are considered the primary factors that influence lidar intensity (Jutzi and Gross 2009; Kaasalainen et al. 2011; Kaasalainen, Kaartinen, and Kukko 2008; Kashani et al. 2015; Sanchiz-Viel et al. 2021; Yan and Shaker 2018; Zhang et al. 2020).

2.2.2. Application

The initial steps in the lidar intensity correction include a series of filtering with each flight line processed individually. First, lidar data were filtered to scan angles of ±15° in accordance with the assumption that snow is primarily forward scattering in the near-infrared wavelengths, but is nearly a Lambertian scatterer near nadir (Donahue, Skiles, and Hammonds 2021; T. H. Painter and Dozier 2004). Next, to best represent the snow surface, the lidar point cloud is filtered to include only single ground returns (Figure 2). Lidar points with more than one return have a diminished intensity value after encountering multiple objects and do not solely

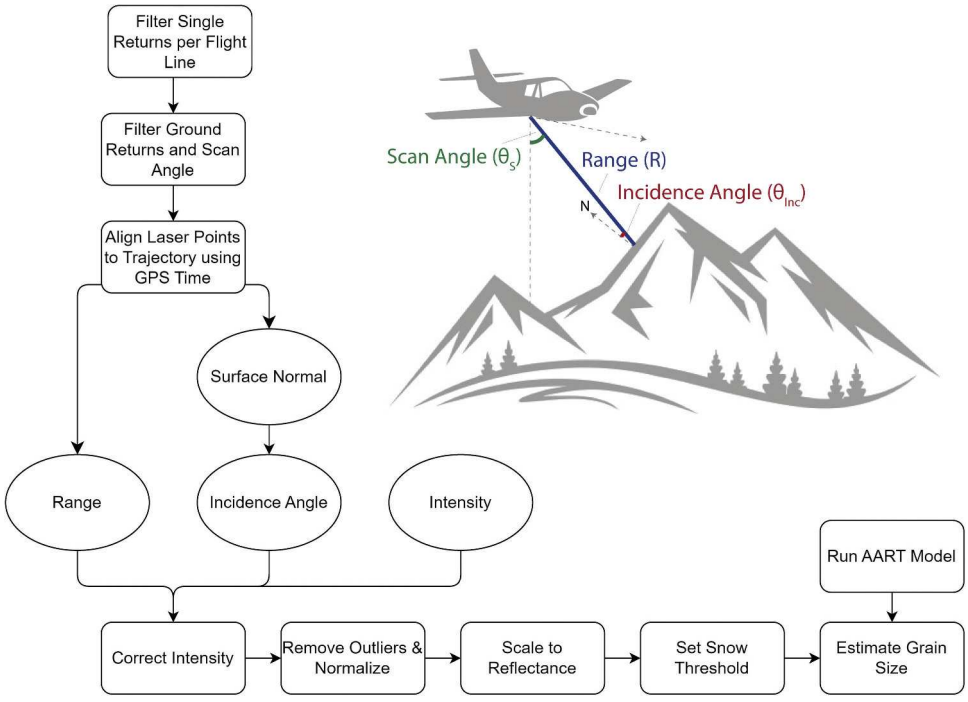

Figure 2. Overview of the methodology that includes calculating the range (R) and the incidence angle (θ_{Inc}, in reference to N or the surface normal) before correcting lidar intensity and estimating snow grain size.

represent light interaction with the snow surface (Kashani et al. 2015). Lastly, to further reduce noise, the point cloud is passed through the extended local minimum (ELM) filter and a voxel centroid nearest neighbor filter, both of which evaluate lidar points in relation to neighboring values and remove outliers that exceed the set threshold (Chen et al. 2012).

In order to correct for the range and incidence angle over mountainous terrain, the relation between the location of the laser scanner and a given laser pulse needs to be determined. We aligned the instantaneous location of the scanner with a given laser pulse by minimizing the GPS time recorded in the aircraft flight trajectory and the time stamp of a given laser pulse. Using these two positions, we calculate the range between the sensor (X_S, Y_S, Z_S) and the ground (X_G, Y_G, Z_G):

$$R = \sqrt{(X_S - X_G)^2 + (Y_S - Y_G)^2 + (Z_S - Z_G)^2} \quad (2.6.)$$

The surface normal (n_1, n_2, n_3) is then calculated using eigenvectors based on the k-nearest neighbors. Both the surface normal and the vector of the laser signal (-*X*, -*Y*, -*Z*) can then be used to calculate the incidence angle of a given laser pulse (Wu et al. 2021):

$$\cos\theta_{inc} = \frac{(-X)\cdot n_1 + (-Y)\cdot n_2 + (-Z)\cdot n_3}{\sqrt{(-X)^2 + (-Y)^2 + (-Z)^2}\cdot\sqrt{{n_1}^2 + {n_2}^2 + {n_3}^2}} \quad (2.7.)$$

We excluded laser signals where incidence angles would exceed 60° as errors in overcorrecting lidar intensity can occur when incidence angles are exceptionally steep (Yan and Shaker 2014), and further tested the sensitivity of retrievals to lower threshold values using 10° increments from 10° to 60°. The calculated range and incidence angle are then required to rectify the raw intensity (I_R) to determine the corrected intensity (I_C) (Kashani et al. 2015):

$$I_C = I_R * \frac{R^2}{R_{ref}^2} * \frac{1}{cos\alpha_i} \quad (2.8.)$$

The reference range (R_{ref}) is a user-defined metric chosen to normalize the data, in which the minimum range or median range are often selected (Yan and Shaker 2017). The median range was applied here as the reference range before removing global outliers that are three standard deviations from the median. To assess sensitivity to the reference range value, it was perturbed by ±10% to represent reasonable uncertainty bounds in determining the median range, which did

not impact the retrieved I_c. The point cloud was then normalized by dividing the maximum corrected intensity before producing the final rasterized 1-m corrected intensity product. We note that the workflow described here is open access, and the link is provided in the code availability section.

2.3. Snow retrievals

Corrected intensity can be converted to reflectance values through radiative transfer modeling if the specifications of the lidar instrumentation are known, but because lidar units are typically proprietary, the sensor information needed for this approach is rarely available, as was the case here. Corrected intensity was instead converted to reflectance using the known reflectance of surfaces within the scene. Here, reflectance at 1064 nm from coincident field spectroscopy measurements of geolocated road asphalt and snow albedo was used to convert the corrected intensity to reflectance. A simple threshold was then used to classify snow-covered area based upon the lowest expected reflectance value for snow (0.30) at 1064 nm (Painter et al. 2009).

We retrieved snow grain size by relating the lidar-derived reflectance and incidence angle to simulated values from the Asymptotic Analytical Radiative Transfer (AART) model (Kokhanovsky and Zege 2004). A range of effective grain radii (30–1500 μm) and incidence angles (0–60°) run through AART yielded a multi-dimensional lookup table of snow reflectance values at 1064 nm. The AART model simulates multiple scattering and reflectance from ice fractals using geometric optics, which has been observed to be a more accurate approach in representing light interactions with snow grains relative to the commonly used spherical models, particularly for new snow. Because the AART model also simulates reflectance in correspondence with observed bidirectional reflectance of snow, it allows for modeling reflectance in the backscatter direction as needed with lidar intensity. Both the lidar-derived reflectance and incidence angle are then referenced to determine grain size across the study site.

The lidar retrieved grain size was then compared against a well-established retrieval approach from measured snow spectral reflectance. The scaled band depth, or the depth of the continuum normalized ice absorption feature centered at 1030 nm, was calculated for each ASD measurement along the reflectance transects (Clark and Roush 1984; Donahue et al. 2023). The grain size was then retrieved by relating the measured scaled band depth to values in a lookup table. The lookup table was produced by simulating spectral reflectance with the AART model over a wide range of grain sizes for the solar geometry at the time of field spectroscopy measurements. Our approach to assess lidar grain size leverages the relative depth of the ice absorption feature as opposed to an absolute reflectance magnitude, an approach that is less sensitive to view and illumination angles (Donahue et al. 2023). The mean grain size values from both the lidar and ASD over the two study sites were used to model snow albedo using the AART model, in order to translate error in grain size to error in snow albedo. The AART model is open access, and a link to the code is provided in the code availability section.

3. Results

3.1. Corrected intensity

The Senator Beck Basin intensity correction offered several improvements relative to the initial (raw) lidar intensity data. The range effect, for instance, was dominant in the raw lidar intensity data as shorter ranges at higher elevations generated larger intensity retrievals. The corrected lidar intensity successfully removed this effect and produced reflectance across the study area independent of the surface elevation (Figure 3). The corresponding median lidar-derived reflectance was 0.68 (0.10 standard deviation), a bright value for 1064 nm consistent with the freshly fallen snow that occurred prior to the lidar flight. The median lidar reflectance held consistent across varying incidence angle thresholds with a maximum increase of 0.02 when the threshold was set to 10° (Table 1). Nevertheless, overcorrection was evident on steep slopes, where a low bias in reflectance was visually prominent as darker areas in the reflectance map relative to surrounding values (Figure 3). The bias effect of steep incidence angles was minimized when the plane directly passed over steep terrain, suggesting that careful adjustments to the flight plan could mitigate this problem as the scan angle is decreased and more retrievals are collected near nadir.

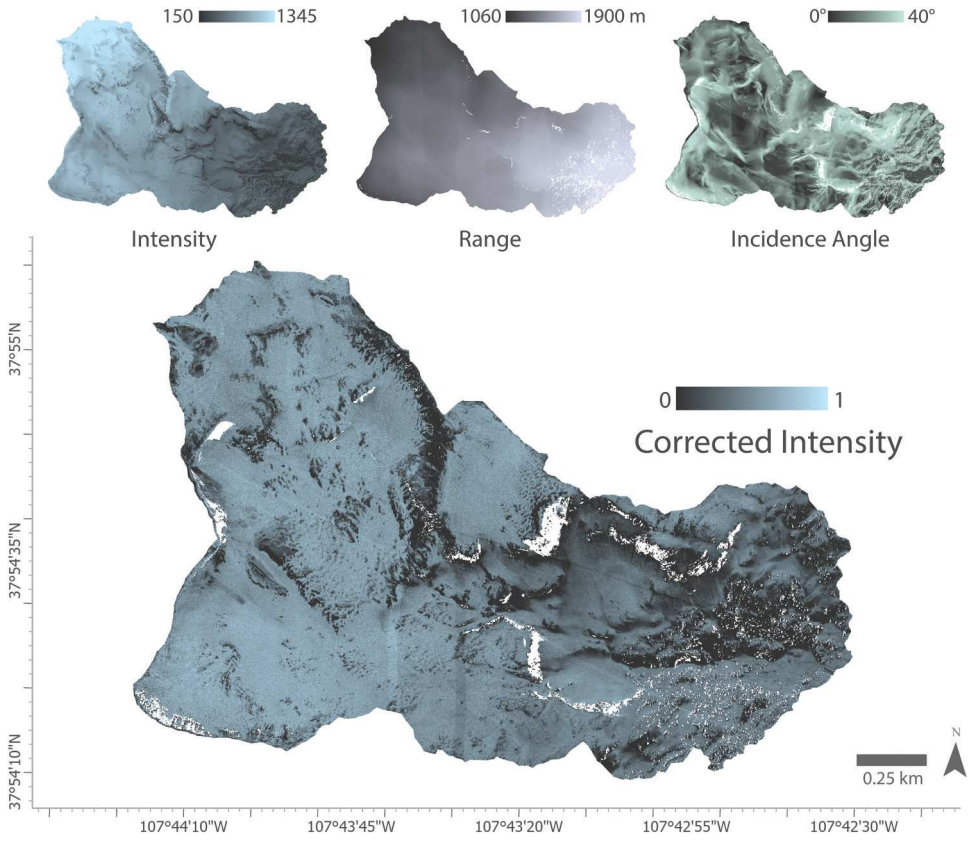

Figure 3. The three parameters needed for intensity correction: raw lidar intensity (top left), range (top center) and incidence angle (top right), including the final corrected lidar intensity (bottom center). Both the incidence angle and the final corrected lidar intensity demonstrate the 40° incidence angle threshold.

Table 1. The range in lidar snow-covered area (km^2), reflectance, and effective grain size (μm) across varying incidence angle thresholds (0–60°).

		Reflectance		Grain Size (μm)	
Incidence Angle Threshold (°)	SCA (km^2)	Median	SD	Median	SD
10	0.97	0.70	0.09	162	101
20	1.86	0.69	0.09	170	114
30	2.57	0.69	0.10	177	128
40	2.88	0.68	0.10	183	123
50	2.94	0.68	0.10	189	155
60	2.96	0.68	0.10	193	168

3.2. Snow extent

The snow cover classification extent was 2.88 km^2 from lidar intensity relative to 2.72 km^2 from imagery (NDSI), a difference of approximately 0.16 km^2 or 5.4% of the total basin area (Figure 4). Snow cover classifications from both the lidar intensity and the imaging spectrometer mapped snow in relatively flat terrain without any overhead obstruction, such as vegetation. However, the snow classification derived from lidar intensity covered a greater extent as it could also identify snow in shadowed areas and around trees, which the imaging spectrometer often misclassified. By lowering the incidence angle threshold to reduce artifacts of overcorrection, the delineated snow extent reduced over slopes (Table 1). For example, at 40° the mapped area decreased by 0.06 km^2 or 2.03% of the total area.

3.3. Snow grain size

Across the entire basin, the median lidar grain size was 183 μm (123 μm standard deviation). The grain size spatial distribution displayed an inverse pattern to corrected intensity, indicative of the relationship

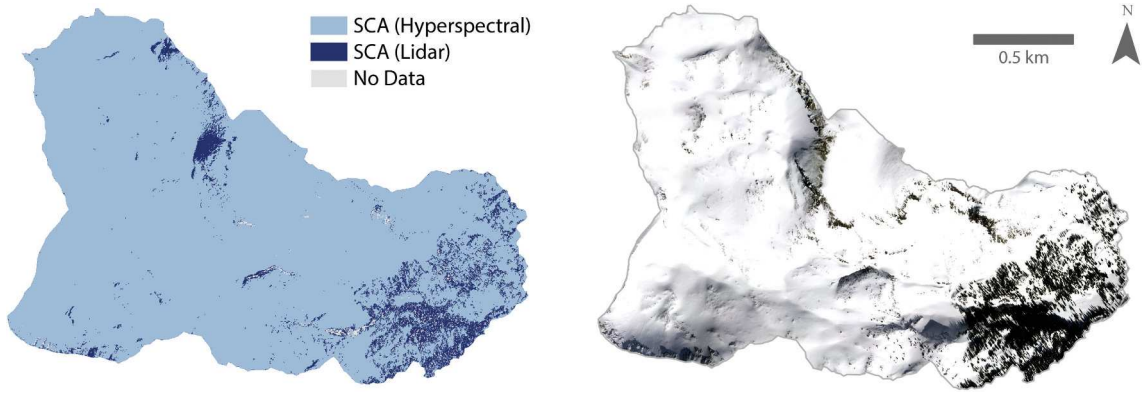

Figure 4. Snow-covered area as determined from an imaging spectrometer (NDSI) and lidar sensor (left) with reference to the orthophoto from the same day of overflight (right). The lidar detected the same snow cover classified from the spectrometer imagery, while also detecting snow in areas not detected by imagery (dark blue). For reference to other maps, lidar snow cover extent is shown for 40° incidence angle.

between near-infrared absorption and snow grain size. At the higher elevation ground measurement sites, the median lidar grain size was 141 µm (MB; Mid-basin) and 126 µm (SBSP; Senator Beck Study Plot), respectively. The median grain size derived from the ASD field spectrometer was 115 µm for the MB transects and 146 µm near the SBSP transects (Figure 5). The transects were measured first at MB and then later in the day at SBSP, so the larger grain sizes were not unexpected. Relative to the in situ grain size, the mean absolute error (MAE) in lidar grain size was 32 µm for both the MB and SBSP transects, which would translate into an albedo uncertainty of ±0.01 (1%).

This error can also apply to absorbed (net) solar radiation (i.e. the primary metric of interest for snow energy balance) as demonstrated here for context. For clean snow, a grain size of 183 µm

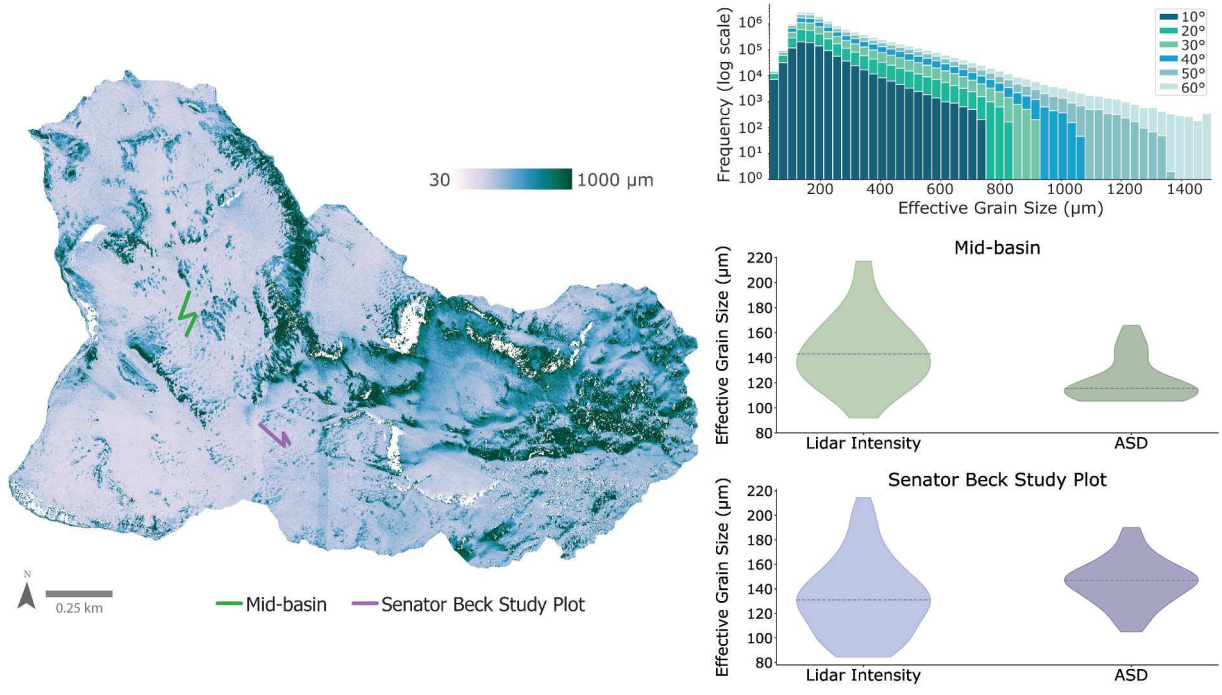

Figure 5. Lidar-derived grain size across the study area with a 40° incidence angle threshold applied, including the transects where in situ measurements were collected (left). Histogram of lidar-derived grain size across the total basin across varying incidence angle thresholds (top right), and associated plots relating grain size from lidar intensity to in situ observations at mid-basin (center right) and Senator Beck Study Plot (lower right).

would translate to a broadband albedo of 0.83. Using a typical incoming solar radiation for this location during time of overflight in mid-February (e.g. 500 W m^{-2}), the absorbed solar radiation would be 85 Wm^{-2}. Perturbing the albedo by ±1% changes absorbed solar radiation by ±5 Wm^{-2}. We note that the relationship between grain size and albedo is non-linear (Dozier and Painter 2004)) and the associated albedo and absorbed solar radiation uncertainty would be lower for larger grained snow with the same MAE. For example, at 500 µm the albedo error would be 0.1%.

Considering that there are differences in retrieval methods and footprint sizes, this initial comparison indicates that lidar-retrieved grain size values were reasonable. The MAE across both transect sites remained consistent (32 µm) across varying incidence angle thresholds; however, the basin median grain size ranged from 162 µm to 193 µm for the 10° and 60° thresholds, respectively (Table 1). Due to the high grain size bias introduced at steep incidence angles, we suggest a 40° incident angle threshold for grain size analysis. Although it is used as the reference measurement here, we note that there is also uncertainty in the grain size retrieved from ground reflectance measurements. The reported sensitivity to variability in environmental conditions is 20 µm (Skiles and Painter 2017). We refer interested readers to further discussion of uncertainties in Donahue, Skiles, and Hammonds (2021) and Skiles et al. (2023).

As an additional assessment of lidar grain size, distributions were examined across the subalpine Swamp Angel Study Plot, where the incidence angle was approximately 0° and inherently had the lowest uncertainty. The median grain size across the meadow encompassing the study plot was 198 µm with a standard deviation of 26 µm. This range of values was reasonable relative to variability in snow grain size mapped from a UAV imaging spectrometer over the same area in March 2022, which had a mean grain size of 100 µm and standard deviation of 23 µm (Skiles et al. 2023). Further assessment of lidar grain size across different snow conditions and on varying slopes is needed before uncertainties can be better constrained, but the initial results here are promising and motivate further assessment of this method and exploration of applications.

4. Discussion

The primary goal of this work was to present a correction workflow for lidar intensity in mountainous terrain. The intensity correction demonstrated the value of correcting for range and incidence angle to retrieve a signal representative of the surface. However, it also showed that high incidence angles were overcorrected, which was more evident when deriving snow grain size. This can be addressed in part by applying an incidence angle threshold, but there is a tradeoff between reducing overcorrection and excluding terrain. Additionally, snow tends to be shallower on steep slopes, which influences the snow metamorphism that could lead to faster grain growth. Thus, it is a challenge to quantitatively identify the bias due to overcorrection alone.

Future work should include sensitivity analysis across steeper slopes (e.g. from coincident airborne VIR-SWIR imaging spectroscopy) to examine the variability in grain size and better interpret the impact of high incidence angles. The overcorrection will be a primary challenge to address for lidar intensity retrievals in mountains, although flight planning and processing workflows could potentially be optimized to limit overcorrection effects. Nevertheless, the uncertainty in absorption (1%) is well under the 10% target identified to improve surface radiation balance in the most recent National Academies' Decadal Survey on Earth Science and Applications (2019).

An additional challenge related to the approach presented here is the empirical conversion of lidar intensity to reflectance. Without coincident field spectroscopy, a reference surface with known reflectance properties at the lidar wavelength within the flight area could be used. This could be a stable snow-free surface such as a road (as used in this study) or rock outcropping. In the absence of these, a reflectance target within the scene could also be utilized. Alternatively, a system calibration effort could be undertaken to establish the relationship between lidar intensity and reflectance. This would be ideal for survey platforms that regularly collect data over similar land surface types using relatively consistent flight parameters (i.e. like ASO), where the relationship is unlikely to change. The accuracy and consistency of such a calibration would need to be assessed across multiple flights. If suitable, however, it would eliminate the need for flight-to-flight conversion from lidar intensity to reflectance and make application of this approach more practical.

The benefit of snow surface property retrievals for a stand-alone lidar platform is clear. Snow surface elevations could be supplemented with snow extent delineated from lidar reflectance, which could be used as a mask to determine where the snow depth should be differentially calculated. The evolution of grain size over time is an indicator of snow age and, via its control on albedo and absorbed solar radiation, could be useful for understanding snow evolution if the dataset was being collected as a time series. An additional step in the workflow could include producing a clean snow albedo map, which could be directly useful to inform change in surface energy balance (Skiles et al. 2023). This methodology could also be applied to other platforms beyond aerial lidar, including ground-based, UAV, and satellite, such as the Global Ecosystem Dynamics Investigation (GEDI) lidar.

Lidar intensity and reflectance could also be a useful supplementary dataset for airborne platforms that couple a lidar with an imaging spectrometer, like ASO (T. H. Painter et al. 2016) or ACO (the Airborne Coastal Observatory; Donahue et al. 2023). With these systems, data collection is often restricted to ideal conditions for optical imaging (e.g. high sun angles, consistent illumination, clear atmosphere) that can pose several challenges for acquiring snow surface properties. For instance, shadows from both terrain and vegetation decrease snow reflectance in optical imagery, particularly in the mountains during winter and spring when sun angles are low (Prantl et al. 2017; Yan and Shaker 2017). Because a lidar system is an active sensor, it can detect snow cover in the presence of thin clouds, in shadowed regions, and over bright snow surfaces. Additionally, because it has a finer spatial resolution, it is better at detecting snow adjacent to trees and other vegetation. Lidar intensity may also have the potential to detect snow cover under tree canopies if last returns are included in the analysis, although the reduction in intensity from the previous returns would also need to be evaluated. Retrieving snow extent and grain size from aerial lidar intensity, therefore, is advantageous as data collection may occur independent of solar illumination, allowing for snow retrievals regardless of the time of day or time of year in the high latitudes. Additionally, snow retrievals are challenging from imagery when pixels are mixed, a common issue in mountain environments. Supplementing imaging spectroscopy retrievals with those from lidar intensity, therefore, may provide more flexibility in regard to illumination conditions and finer surface detail at the point cloud level.

5. Conclusion

Aerial lidar intensity at 1064 nm has proven to be a valuable alternative for retrieving snow surface properties, including extent and grain size, after correcting for range and incidence angle. The lidar-derived grain size demonstrated a mean absolute error (MAE) of 32 µm relative to in situ measurements, corresponding to an uncertainty of 1% in snow albedo and absorption. This approach, utilizing only one wavelength, exhibited greater variability than field spectroscopy, particularly on steeper slopes where incidence angles were high. To mitigate this, we recommend incorporating an incidence angle threshold and recognize that coincident field spectroscopy would also facilitate the conversion of lidar intensity to reflectance. Despite these challenges, lidar intensity corrections are still a useful supplement to traditional methods, as lidar can detect snow surfaces at finer resolutions and is independent of solar illumination, which is especially useful around vegetation and in shadows. Further assessment of this methodology across varying snow conditions and slopes is recommended, as well as its application across different lidar platforms, such as UAVs or satellites. Although this technique has its limitations, it holds great potential to enhance current methods for monitoring snow evolution and energy balance.

Acknowledgments

The authors would like to recognize the NASA-JPL Airborne Snow Observatory and NASA SnowEx 2017 for their collection of the aerial lidar data, and Dr Jewell Lund for assistance collecting in situ albedo and reflectance measurements.

Disclosure statement

No potential conflict of interest was reported by the author(s).

Funding

This work was supported by NASA Project 80NSSC22K0686, NSF Award 2012091, and NOAA via the Cooperative Institute for Research to Operations in Hydrology (CIROH) project NA22NWS4320003.

ORCID

Christopher P. Donahue http://orcid.org/0000-0002-4585-6908
Brian Menounos http://orcid.org/0000-0002-3370-4392
S. McKenzie Skiles http://orcid.org/0000-0002-7726-6355

Author contributions statement

CA and MS produced the concept and methodology; MS collected field data and acquired funding; CA and BM developed the code; CA, MS, and CD analyzed and interpreted the results; CA wrote the initial draft; MS, CD, and BM revised the written content; all authors agree to be accountable for each aspect of this research.

Data and code availability

The workflow presented here can be accessed on GitHub (https://GitHub.com/UofU-Cryosphere/lidar-intensity-correction) and the datasets used here can be accessed on Zenodo (https://doi.org/10.5281/zenodo.12701606). More broadly, ASO and SnowEx data are publicly available on the National Snow and Ice Data Center (https://nsidc.org/data/snowex and https://nsidc.org/data/aso).

References

Antonarakis, A. S., K. S. Richards, and J. Brasington. 2008. "Object-Based Land Cover Classification Using Airborne LiDAR. *Remote Sensing of Environment*." *Remote Sensing of Environment* 112 (6): 2988–2998. https://doi.org/10.1016/j.rse.2008.02.004.

Anttila, K., T. Hakala, S. Kaasalainen, H. Kaartinen, O. Nevalainen, A. Krooks, and A. Jaakkola. 2016. "Calibrating Laser Scanner Data from Snow Surfaces: Correction of Intensity Effects." *Cold Regions Science & Technology* 121:52–59. https://doi.org/10.1016/j.coldregions.2015.10.005.

Arnold, N., W. Rees, B. Devereux, and G. Amable. 2006. "Evaluating the Potential of High-Resolution Airborne LIDAR Data in Glaciology." *International Journal of Remote Sensing* 27 (6): 1233–1251. https://doi.org/10.1080/01431160500353817.

Baltsavias, E. P. 1999. "Airborne Laser Scanning: Basic Relations and Formulas." *Isprs Journal of Photogrammetry & Remote Sensing* 54 (2): 199–214. https://doi.org/10.1016/S0924-2716(99)00015-5.

Bhardwaj, A., L. Sam, A. Bhardwaj, and F. J. Martín-Torres. 2016. "LiDAR Remote Sensing of the Cryosphere: Present Applications and Future Prospects." *Remote Sensing of Environment* 177:125–143. https://doi.org/10.1016/j.rse.2016.02.031.

Bretagne, E., P. Dassonvalle, and G. Caron. 2018. "Spherical Target-Based Calibration of Terrestrial Laser Scanner Intensity. Application to Colour Information Computation." *Isprs Journal of Photogrammetry & Remote Sensing* 144:14–27. https://doi.org/10.1016/j.isprsjprs.2018.06.014.

Chen, Z., B. Devereux, B. Gao, and G. Amable. 2012. "Upward-Fusion Urban DTM Generating Method Using Airborne Lidar Data." *Isprs Journal of Photogrammetry & Remote Sensing* 72:121–130. https://doi.org/10.1016/j.isprsjprs.2012.07.001.

Clark, R. N., and T. L. Roush. 1984. "Reflectance Spectroscopy: Quantitative Analysis Techniques for Remote Sensing Applications." *Journal of Geophysical Research: Solid Earth* 89 (B7): 6329–6340. https://doi.org/10.1029/JB089iB07p06329.

Currier, W. R., J. Pflug, G. Mazzotti, T. Jonas, J. S. Deems, K. J. Bormann, and J. D. Lundquist. 2019. "Comparing Aerial Lidar Observations with Terrestrial Lidar and Snow-Probe Transects from NASA's 2017 SnowEx Campaign." *Water Resources Research* 55 (7): 6285–6294. https://doi.org/10.1029/2018WR024533.

Deems, J. S., S. R. Fassnacht, and K. J. Elder. 2006. "Fractal Distribution of Snow Depth from LiDAR Data." *Journal of Hydrometeorology* 7 (2): 285–297. https://doi.org/10.1175/JHM487.1.

Deems, J. S., T. H. Painter, and D. C. Finnegan. 2013. "Lidar Measurement of Snow Depth: A Review." *Journal of Glaciology* 59 (215): 467–479. https://doi.org/10.3189/2013JoG12J154.

Donahue, C. P., B. Menounos, N. Viner, S. M. Skiles, S. Beffort, T. Denouden, and D. Heathfield. 2023. "Bridging the Gap Between Airborne and Spaceborne Imaging Spectroscopy for Mountain Glacier Surface Property Retrievals." *Remote Sensing of Environment* 299:113849. https://doi.org/10.1016/j.rse.2023.113849.

Donahue, C. P., S. M. Skiles, and K. Hammonds. 2021. "In situ Effective Snow Grain Size Mapping Using a Compact Hyperspectral Imager." *Journal of Glaciology* 67 (261): 49–57. https://doi.org/10.1017/jog.2020.68.

Dozier, J., and T. H. Painter. 2004. "Multispectral and Hyperspectral Remote Sensing of Alpine Snow Properties." *Annual Review of Earth and Planetary Sciences* 32 (1): 465–494. https://doi.org/10.1146/annurev.earth.32.101802.120404.

Goodwin, N. R., N. C. Coops, and D. S. Culvenor. 2006. "Assessment of Forest Structure with Airborne LiDAR and the Effects of Platform Altitude." *Remote Sensing of Environment* 103 (2): 140–152. https://doi.org/10.1016/j.rse.2006.03.003.

Hartzell, P. J., P. J. Gadomski, C. L. Glennie, D. C. Finnegan, and J. S. Deems. 2015. "Rigorous Error Propagation for Terrestrial Laser Scanning with Application to Snow Volume Uncertainty." *Journal of Glaciology* 61 (230): 1147–1158. https://doi.org/10.3189/2015JoG15J031.

Helfricht, K., M. Kuhn, M. Keuschnig, and A. Heilig. 2014. "Lidar Snow Cover Studies on Glaciers in the Ötztal Alps (Austria): Comparison with Snow Depths Calculated from GPR Measurements." *The Cryosphere* 8 (1): 41–57. https://doi.org/10.5194/tc-8-41-2014.

Höfle, B., and N. Pfeifer. 2007. "Correction of Laser Scanning Intensity Data: Data and Model-Driven Approaches." *Isprs Journal of Photogrammetry & Remote Sensing* 62 (6): 415–433. https://doi.org/10.1016/j.isprsjprs.2007.05.008.

Hood, J. L., and M. Hayashi. 2010. "Assessing the Application of a Laser Rangefinder for Determining Snow Depth in Inaccessible Alpine Terrain." *Hydrology and Earth System Sciences* 14 (6): 901–910. https://doi.org/10.5194/hess-14-901-2010.

Jelalian, A. 1992. *Laser Radar Systems*. Norwood, MA, USA: Artech House on Demand.

Jutzi, B., and H. Gross. 2009. "Normalization of LiDAR Intensity Data Based on Range and Surface Incidence Angle." In *Proceedings of Laserscanning 2009*, Paris, France, Septembe 1–2, 2009, 213–218. Vol. 38. In IAPRS.

Kaasalainen, S., A. Jaakkola, M. Kaasalainen, A. Krooks, and A. Kukko. 2011. "Analysis of Incidence Angle and Distance Effects on Terrestrial Laser Scanner Intensity: Search for Correction Methods." *Remote Sensing* 3 (10): 2207–2221. https://doi.org/10.3390/rs3102207.

Kaasalainen, S., H. Kaartinen, and A. Kukko. 2008. "Snow Cover Change Detection with Laser Scanning Range and Brightness Measurements." EARSeL eProceedings (9): 133–141. http://www.eproceedings.org/static/vol07_2/07_2_kaasalainen1.pdf.

Kashani, A. G., M. J. Olsen, C. E. Parrish, and N. Wilson. 2015. "A Review of Lidar Radiometric Processing: From Ad Hoc Intensity Correction to Rigorous Radiometric Calibration." *Sensors* 15 (11): 28099–28128. https://doi.org/10.3390/s151128099.

Kokhanovsky, A. A., and E. P. Zege. 2004. "Scattering Optics of Snow. *Applied Optics*." *Applied Optics* 43 (7): 1589–1602. https://doi.org/10.1364/AO.43.001589.

Landry, C. C., K. A. Buck, M. S. Raleigh, and M. P. Clark. 2014. "Mountain System Monitoring at Senator Beck Basin, San Juan Mountains, Colorado: A New Integrative Data Source to Develop and Evaluate Models of Snow and Hydrologic Processes [https://doi.org/10.1002/2013WR013711]." *Water Resources Research* 50 (2): 1773–1788. https://doi.org/10.1002/2013WR013711.

Lang, M. W., and G. W. McCarty. 2009. "Lidar Intensity for Improved Detection of Inundation Below the Forest Canopy." *Wetlands* 29 (4): 1166–1178. https://doi.org/10.1672/08-197.1.

Lutz, E. R., T. Geist, and J. Stötter. 2003. "Investigations of airborne laser scanning signal intensity on glacial surfaces– Utilizing comprehensive laser geometry modelling and orthophoto surface modelling (A case study: Svartisheibreen, Norway)." In Proceedings, ISPRSWorkshopon3-Dreconstruction fromairborne laserscanner and INSAR data, Dresden, Germany.

Mott, R., M. Schirmer, and M. Lehning. 2011. "Scaling Properties of Wind and Snow Depth Distribution in an Alpine Catchment [https://doi.org/10.1029/2010JD014886]." *Journal of Geophysical Research Atmospheres* 116 (D6): 116. https://doi.org/10.1029/2010JD014886.

National Academies of Sciences, Division on Engineering, Physical Sciences, Space Studies Board, Committee on the Decadal Survey for Earth Science, & Applications from Space. 2019. *Thriving on Our Changing Planet: A Decadal Strategy for Earth Observation from Space*. Washington, D.C., USA: National Academies Press.

Nolin, A. W. 1998. "Mapping Snow Grain Size on the Ice Sheets with a Laser Altimeter." In *Proceedings of the IEEE International Geoscience and Remote Sensing (IGARSS '98) Symposium on Sensing and Managing the Environment*, Seattle, WA, USA, July 6–10, 1998, 2264–2266. Vol. 4.

Painter, T. H., D. Berisford, J. Boardman, K. Bormann, J. Deems, F. Gehrke, and A. Winstral. 2016. "The Airborne Snow Observatory: Fusion of Scanning Lidar, Imaging Spectrometer, and Physically-Based Modeling for Mapping Snow Water Equivalent and Snow Albedo." *Remote Sensing of Environment* 184:139–152. https://doi.org/10.1016/j.rse.2016.06.018.

Painter, T. H., and J. Dozier. 2004. "Measurements of the Hemispherical-Directional Reflectance of Snow at Fine Spectral and Angular Resolution." *Journal of Geophysical Research Atmospheres* 109 (D18). https://doi.org/10.1029/2003JD004458.

Painter, T. H., K. Rittger, C. McKenzie, P. Slaughter, R. E. Davis, and J. Dozier. 2009. "Retrieval of Subpixel Snow Covered Area, Grain Size, and Albedo from MODIS." *Remote Sensing of Environment* 113 (4): 868–879. https://doi.org/10.1016/j.rse.2009.01.001.

Painter, T. H., F. C. Seidel, A. C. Bryant, S. McKenzie Skiles, and K. Rittger. 2013. "Imaging Spectroscopy of Albedo and Radiative Forcing by Light-Absorbing Impurities in Mountain Snow." *Journal of Geophysical Research Atmospheres* 118 (17): 9511–9523. https://doi.org/10.1002/jgrd.50520.

Prantl, H., L. Nicholson, R. Sailer, F. Hanzer, I. F. Juen, and P. Rastner. 2017. "Glacier Snowline Determination from Terrestrial Laser Scanning Intensity Data." *Geosciences* 7 (3): 60. https://doi.org/10.3390/geosciences7030060.

Prokop, A. 2008. "Assessing the Applicability of Terrestrial Laser Scanning for Spatial Snow Depth Measurements." *Cold Regions Science & Technology* 54 (3): 155–163. https://doi.org/10.1016/j.coldregions.2008.07.002.

Sanchiz-Viel, N., E. Bretagne, E. M. Mouaddib, and P. Dassonvalle. 2021. "Radiometric Correction of Laser Scanning Intensity Data Applied for Terrestrial Laser Scanning." *Isprs Journal of Photogrammetry & Remote Sensing* 172:1–16. https://doi.org/10.1016/j.isprsjprs.2020.11.015.

Skiles, S. M., C. Donahue, A. Hunsaker, and J. Jacobs. 2023. "UAV Hyperspectral Imaging for Multiscale Assessment of Landsat 9 Snow Grain Size and Albedo." *Frontiers in Remote Sensing* 3:110. https://doi.org/10.3389/frsen.2022.1038287.

Skiles, S. M., and T. Painter. 2017. "Daily Evolution in Dust and Black Carbon Content, Snow Grain Size, and Snow Albedo During

Snowmelt, Rocky Mountains, Colorado." *Journal of Glaciology* 63 (237): 118–132. https://doi.org/10.1017/jog.2016.125 .

Soffer, R., National Research Council Canada. 2021. "Lab-Based Spectroradiometric Validation of FRL VNIR Imaging Spectrometers. National Research Council Canada [Conseil national de recherches Canada]. https://doi.org/10.4224/9780660371375.

Song, J.-H., S.-H. Han, K. Yu, and Y.-I. Kim. 2002. "Assessing the Possibility of Land-Cover Classification Using Lidar Intensity Data." *International Archives of Photogrammetry, Remote Sensing and Spatial Information Sciences* 34 (3/B): 259–262.

Soudarissanane, S., R. Lindenbergh, M. Menenti, and P. Teunissen. 2009. "Incidence Angle Influence on the Quality of Terrestrial Laser Scanning Points." In *Proceedings ISPRS Workshop Laserscanning 2009*, Paris, France. 1–2Sept 2009.

Vionnet, V., C. B. Marsh, B. Menounos, S. Gascoin, N. E. Wayand, J. Shea, K. Mukherjee, and J. W. Pomeroy. 2021. "Multi-Scale Snowdrift-Permitting Modelling of Mountain Snowpack." *The Cryosphere* 15 (2): 743–769. https://doi.org/10.5194/tc-15-743-2021.

Warren, S. G. 1982. "Optical Properties of Snow." *Reviews of Geophysics* 20 (1): 67–89. https://doi.org/10.1029/RG020i001p00067.

Wu, Q., R. Zhong, P. Dong, Y. Mo, and Y. Jin. 2021. "Airborne Lidar Intensity Correction Based on a New Method for Incidence Angle Correction for Improving Land-Cover Classification." *Remote Sensing* 13 (3): 511. https://doi.org/10.3390/rs13030511.

Yan, W. Y., and A. Shaker. 2014. "Radiometric Correction and Normalization of Airborne Lidar Intensity Data for Improving Land-Cover Classification." *IEEE Transactions on Geoscience & Remote Sensing* 52 (12): 7658–7673. https://doi.org/10.1109/TGRS.2014.2316195.

Yan, W. Y., and A. Shaker. 2017. "Correction of Overlapping Multispectral Lidar Intensity Data: Polynomial Approximation of Range and Angle Effects." *International Archives of the Photogrammetry, Remote Sensing and Spatial Information Sciences* XLII-3/W1:177–182. https://doi.org/10.5194/isprs-archives-XLII-3-W1-177-2017.

Yan, W. Y., and A. Shaker. 2018. "Airborne Lidar Intensity Banding: Cause and Solution." *Isprs Journal of Photogrammetry & Remote Sensing* 142:301–310. https://doi.org/10.1016/j.isprsjprs.2018.06.013.

Yang, Y., A. Marshak, M. Han, S. P. Palm, and D. J. Harding. 2017. "Snow Grain Size Retrieval Over the Polar Ice Sheets with the Ice, Cloud, and Land Elevation Satellite (ICESat) Observations." *Journal of Quantitative Spectroscopy & Radiative Transfer* 188:159–164. https://doi.org/10.1016/j.jqsrt.2016.03.033.

Zhang, C., S. Gao, W. Li, K. Bi, N. Huang, Z. Niu, and G. Sun. 2020. "Radiometric Calibration for Incidence Angle, Range and Sub-Footprint Effects on Hyperspectral Lidar Backscatter Intensity." *Remote Sensing* 12 (17). https://doi.org/10.3390/rs12172855.